Naval Research Laboratory
Washington, DC 20375-5320

NRL/MR/5620--03-8671

Field and Laboratory Boresighting Methods for Hyperspectral Imaging Sensor Systems

FREDERICK M. OLCHOWSKI
CHRISTOPHER M. STELLMAN

Advanced Concepts Branch
Optical Sciences Division

FRANK BUCHOLTZ, CONSULTANT

SFA Inc.
Largo, MD

March 6, 2003

REPORT DOCUMENTATION PAGE

Form Approved
OMB No. 0704-0188

1. REPORT DATE *(DD-MM-YYYY)*	2. REPORT TYPE	3. DATES COVERED *(From - To)*
March 6, 2003		

4. TITLE AND SUBTITLE

Field and Laboratory Boresighting Methods for Hyperspectral Imaging Sensor Systems

5a. CONTRACT NUMBER

5b. GRANT NUMBER

5c. PROGRAM ELEMENT NUMBER

6. AUTHOR(S)

Frederick M. Olchowski, Christopher M. Stellman, and Frank Bucholtz*

5d. PROJECT NUMBER

5e. TASK NUMBER

5f. WORK UNIT NUMBER

7. PERFORMING ORGANIZATION NAME(S) AND ADDRESS(ES)

Naval Research Laboratory
4555 Overlook Avenue, SW
Washington, DC 20375-5320

SFA Inc.
9315 Largo Drive West, Suite 200
Largo, MD 20774

8. PERFORMING ORGANIZATION REPORT NUMBER

NRL/MR/5620--03-8671

9. SPONSORING / MONITORING AGENCY NAME(S) AND ADDRESS(ES)

10. SPONSOR / MONITOR'S ACRONYM(S)

11. SPONSOR / MONITOR'S REPORT NUMBER(S)

12. DISTRIBUTION / AVAILABILITY STATEMENT

Approved for public release; distribution is unlimited.

13. SUPPLEMENTARY NOTES

*SFA Inc., 9315 Largo Dr. West, Suite 200, Largo, MD 20774

14. ABSTRACT

Multi-sensor platforms for airborne reconnaissance and surveillance often require the alignment of two or more imaging systems along a common optical axis. This is true especially when data fusion is performed where the signal processing involves the analysis of data taken from different sensors at the same time and of the same location. For example, the NRL War Horse platform combines imagery from a VIS/NIR slit-dispersive hyperspectral sensor with imagery from a slit-aperture linear CCD array camera with pointing and geolocation information from a digital GPS/INS instrument (C-MIGITS). This sensor suite has flown successfully aboard the Unmanned Air Vehicle (UAV) Predator.

Several crude boresighting procedures have been adopted for use in the field which take advantage of long baselines between the camera systems and objects at a distance. However, accurate alignment procedures are difficult to perform in the field owing to variable and unpredictable hangar, aircraft, and weather conditions. Typically, the various imaging and geolocation instruments are mounted on mechanical frame prior to installation on the aircraft. Hence, it is desirable to have an accurate method for boresighting a suite of sensors to a common optical axis in the laboratory using a relatively short baseline.

15. SUBJECT TERMS

Boresighting; Hyperspectral; Collimation

16. SECURITY CLASSIFICATION OF:			17. LIMITATION OF ABSTRACT	18. NUMBER OF PAGES	19a. NAME OF RESPONSIBLE PERSON
a. REPORT	b. ABSTRACT	c. THIS PAGE			Frederick M. Olchowski
Unclassified	Unclassified	Unclassified	UL	25	19b. TELEPHONE NUMBER *(include area code)* (202) 404-3050

Standard Form 298 (Rev. 8-98)
Prescribed by ANSI Std. Z39.18

CONTENTS

Introduction 1

Statement of the Problem 1

Field Boresighting Method 1

Laboratory Boresighted Method 4

A. Collimated Light Source 4
B. Reflective Method for Laboratory Boresighting 7

Expected Accuracy of Laboratory Boresighting Method 8

Summary 9

FIELD AND LABORATORY BORESIGHTING METHODS FOR HYPERSPECTRAL IMAGING SENSOR SYSTEMS

Introduction

Multi-sensor platforms for airborne reconnaissance and surveillance often require the alignment of two or more imaging systems along a common optical axis. This is true especially when data fusion is performed where the signal processing involves the analysis of data taken from different sensors at the same time and of the same location. For example, the NRL War Horse platform combines imagery from a VIS/NIR slit-dispersive hyperspectral sensor with imagery from a slit-aperture linear CCD array camera with pointing and geolocation information from a digital GPS/INS instrument (C-MIGITS). This sensor suite has flown successfully aboard the Unmanned Air Vehicle (UAV) Predator.

Several crude boresighting procedures have been adopted for use in the field which take advantage of long baselines between the camera systems and objects at a distance. However, accurate alignment procedures are difficult to perform in the field owing to variable and unpredictable hangar, airfield and weather conditions. Typically, the various imaging and geolocation instruments are mounted on a mechanical frame prior to installation on the aircraft. Hence, it is desirable to have an accurate method for boresighting a suite of sensors to a common optical axis in the laboratory using a relatively short baseline.

Statement of the Problem

Figure 1 shows the three angular degrees of freedom of an arbitrary sensor with respect to a fixed reference frame. We consider only the case where all sensors are rigidly mounted to a common mechanical frame, that is, we do not consider sensors on rotary mounts or gimbal stages. We define boresighting as the act of aligning the sensor axis along a particular direction in space. The applications considered here are those in which it is not necessary to boresight all the sensors to a particular direction with respect to either the mechanical frame of the sensors or the aircraft, but rather those applications in which all sensors must only point along a common direction. For practical expediency, then, one of the sensors may be chosen as the "reference" sensor and all the remaining sensors may be boresighted to the reference sensor. Alternatively, for laboratory boresighting, a direction defined by a single collimated beam on the optical bench, for example, may be chosen as the reference direction.

Field Boresighting Method

The field boresighting method described here requires
i) At least one sensor rigidly mounted to the common frame serving as the reference sensor;
ii) at least a 2-axis rotary platform (pan-tilt) capable of holding the entire common frame (a three-axis platform is preferable);

Manuscript approved February 12, 2003.

iii) clear line-of-sight between the sensors and large objects in the far-field containing sharp, observable, easily identifiable vertical and horizontal boundaries (obviously, these are typically man-made structures).

Here we describe the field boresighting procedure used for the War Horse system comprising the War Horse slit-dispersive hyperspectral imager (HSI) and a Dalsa slit-aperture linear CCD array. These two sensors are strictly boresighted when the image planes of the two sensors lie in parallel planes and the relative roll angle between the linear CCD array and any row of pixels of the HSI focal plane array (FPA) (corresponding to the spatial, not spectral, direction) is zero. Parallel image planes means that the relative pitch and yaw angles are zero. (See Fig 1). The mechanical arrangement of this system is such that the HSI is rigidly mounted to the common frame with no angular adjustment of any kind while the Dalsa camera has pitch and yaw adjustment but, unfortunately, no roll adjustment. A proposed method for making roll adjustments will be discussed below.

The two sensors must be mounted so that their slits are oriented not only parallel to each other, but such that the respective FPAs are in the same direction with regard to field of view. That is, the two sensors must be oriented to have common right-to-left fields of view. It should be noted that this state cannot be discerned simply from visual inspection of the slits. However, the orientation is easily checked by moving an object across the field of view of each sensor and verifying that the image on the FPA of each sensor moves in the same direction.

Boresighting proceeds as follows. For clarity, we consider the case of the slits of the two sensors oriented in the vertical direction as shown in Fig. 1.

1) An easily identifiable horizontal boundary in the far field, such as a roof line, is chosen.

2) The pan-tilt stage holding the common frame is adjusted while viewing the HSI output to bring the roofline exactly to the center of the field-of-view. For example, with 512 pixels in the spatial direction, the roofline boundary should be brought to appear at pixel 256. The pan-tilt stage is then locked in place.

At this point, if the mechanical design, machining and construction of the common platform were adequate, the same roofline should be well within the field of view of the Dalsa camera.

3) The appropriate screws holding the Dalsa camera to the frame are adjusted, while viewing the Dalsa output, to bring the same roofline to the exact center of the Dalsa image.

Completing Steps 1-3 ensures that the optical axes of both instruments lie in the xy-plane, but they may still not be parallel.

4) Next, an easily identifiable vertical boundary in the far field, such as a building wall edge, is chosen.

5) The pan-tilt stage is moved to bring the vertical boundary into view, as discerned by the boundary edge moving back-and-forth across the field of view as the pan-tilt stage is rotated back-and-forth in the horizontal plane. The goal in this step is to adjust the Dalsa so that the boundary edge crosses the center of the fields-of-view of the Dals and the HSI sensor at the same instant. By observing whether the crossing of the Dalsa image of the building edge leads ahead of or lags behind the crossing in the HSI, a good guess can be made regarding which way to adjust the Dalsa camera.

6) Adjust the Dalsa camera in small increments while panning back-and-forth to get the two images of the building edge to cross the center of their respective fields of view at the same instant.

Completing Steps 1-6 ensures that the optical axis of both sensors lie along the x-axis of Fig. 1. At this point there is still no guarantee that the relative roll angle between the sensors is zero. Unfortunately, as mentioned above, the War Horse system in its present configuration does not allow adjustment of the roll angle of either sensor with respect to the mounting frame and the full boresighting procedure cannot be completed.

If roll adjustment of the Dalsa were possible, boresighting would be completed as follows.

7) Adjust the pan-tilt stage until the vertical boundary is near the edge of the field of view of the sensor with the smaller field of view (the HSI in this case).

8) Adjust the roll of the Dalsa camera in small increments while again panning back-and-forth but, this time, watching the crossing of the building edge at the extreme edge of the fields-of-view, not the center. Continue until the images of the building edge flash across the edges of the fields of view at the same instant.

This completes the field boresighting procedure. In practice, it is to be expected that there will be some interplay between mechanical adjustments and, hence, the accuracy of the boresighting procedure will be improved by iterating between steps. Extending the procedure to sensor suites involving more than two sensors is straightforward, with each additional sensor boresighted with respect to the reference sensor.

Admittedly, this procedure relies on the judgment of the operator, for example, to decide that images change "simultaneously" on the two cameras. However, it is not unreasonable to expect that the operator can make adjustments and alignments down to the resolution of a few pixels, say p pixels where $1 \leq p \leq 5$. Let $\Delta\rho_{error}$ be the difference between the actual roll angle and the roll angle required for perfect boresight alignment, etc. Then the rms angular accuracy of the boresighting procedure is

$$\beta_{rms} = \text{sqrt}\,[\Delta\rho_{error}^{\ 2} + \Delta\psi_{error}^{\ 2} + \Delta\theta_{error}^{\ 2}\ ] \qquad (1)$$

Assuming equal uncertainty of approximately p pixels for each angular adjustment, the rms angular accuracy of the boresighting procedure is

$$\beta_{rms} = (\sqrt{3}p)*IFOV_{max,} \qquad (2)$$

where $IFOV_{max,}$ is the largest IFOV of the sensors in the suite.

To make a crude estimate, using values for the parameters listed in Table 2, the best case to worst case β_{rms} lies in the range 87 urad (Dalsa at p=1) $\leq \beta_{rms} \leq$ 2420 urad (WarHORSE at p=5). Operational experience suggests that the WarHORSE sensor can be manually aligned to p = 1-2 pixels and, hence, a realistic typical expected alignment may be in the range $\beta_{rms} \sim$ 485-970 urad.

Laboratory Boresighting Method

A. Collimated Light Source

Compared to the field method, a laboratory boresighting procedure typically does not have the luxury of long optical baselines to remove the effects of parallax. However, parallax can be effectively eliminated using collimated light from a nearby source. In this case, the distance between the source(object) and the sensor can be quite small and can be accommodated easily on a standard optical table.

Collimated light is obtained by placing a point source at the focal point of a positive lens as shown in **Fig. 2**. **Figure 3** shows a practical implementation of this approach using an optical fiber and a telescope. For our measurements we chose singlemode optical fiber (Corning SMF28) and a Celestron 14-inch Schmidt-Cassegrain telescope. A custom fiber holder was fabricated (**Fig. 4**) to adapt the fiber chuck (Newport Model FPH-CH4) to the 1.25" eyepiece opening on the telescope. The large telescope aperture allows two sensors to be illuminated simultaneously.

The exit optics of the singlemode fiber are summarized in **Fig. 5**. For this fiber, designed for singlemode operation at 1.5 um wavelength (and longer), the mode field diameter is approximately 10 um and the numerical aperture $NA_f = \sin\theta_f \sim 0.14$ ($\sim$ 8 deg). The effective f/# of this fiber is f/# = $1/(2*NA_f)$ = f/3.8. By contrast, the Celestron telescope is f/11 (NA_t = 0.0455, $\theta_t \sim$ 2.6 deg) with a 3910 mm focal length so only a fraction of the optical power emitted by the fiber will be "captured" and collimated by the telescope. The remaining light will either be scattered within the telescope body or will exit the telescope as non-collimated light. It will be seen that neither of these effects has a

serious deleterious effect on the boresighting procedure. Optical parameters of the fiber and telescope are summarized in Fig. 6 and Table 1.

Table 1

Parameter	Symbol	**SMF28 Fiber**	**14" Celestron Telescope**
Numerical Aperture	NA	0.14	0.046
f/#	f/#	f / 3.8	f / 11
Cone half-angle (deg)	θ	8.0	2.6
Focal length (mm)	*f*	na	1390
Mode field diam (mm)	MFD	10 e -3	na
Diam	D	na	14" = 356mm
Diam Central Obscur.	D'	na	4.5" = 114mm

Notes:

1) na = "not applicable"

2) The diameter of the entrance aperture for the War Horse HSI is Ds = 1.25" = 31.8 mm

We wish to calculate the fraction of optical power emitted from the fiber that reaches the sensor's focal plane array (FPA). Let Pf = optical power exiting the fiber. Then the optical power exiting the telescope, neglecting losses in the telescope (e.g. due to the corrector plate) is

$$Pt = Pf * (NA_t / NA_f)^2 \qquad (3)$$

where NA_t and NA_f are defined above. Here we have neglected the effects of the small obscuration in the primary mirror due to the eyepiece hole. Referring to Figs. 6a and 6b, the maximum amount of light which can be captured by the HSI is proportional to the ratio of the area of the entrance aperture stop of the HSI, As, to the annular area of the telescope, Aa.

$$P_{HSI} = Pt * (As / Aa) \qquad (4)$$

Let D be the diameter of the telescope , D' be the diameter of the telescope's central obscuration, and D_S be the diameter of the HSI entrance aperture (1.25" = 31.8mm). Then

$$Aa = (\pi/4) * [D^2 - D'^2] \qquad (5)$$

and

$$As = (\pi/4) * D_S^2 . \qquad (6)$$

Finally,

$$P_{HSI} = q * Pf \quad (7)$$

where

$$q = (NA_t / NA_f)^2 * [(D_S^2) / (D^2 - D'^2)] . \quad (8)$$

This equation is valid provided $(D-D') \geq D_S$ and Aa>>As. For the values listed in Table 1, $q = (P_{HSI} / Pf) = 9.6$ e -4. That is, approximately one in every thousand photons that leaves the fiber reaches the foreoptics of the HSI.

To determine a reasonable value for Pf we bound the problem by noting that for typical VIS/NIR and SWIR FPAs available today, the maximum well capacity is on the order of a few hundred thousand electrons, while the system noise levels are on the order of 50 - 100 electrons. Therefore, it will be reasonable to adjust Pf such that 50,000 - 100,000 photons reach the FPA during one integration time period.

Assume the collimated light is monochromatic at wavelength λ. Then the photon flux Φ (number of photons per second) contained in a beam of optical power P is

$$\Phi = (\text{Optical power}) / (\text{Average photon energy}) = P / (hc / \lambda) \quad (9)$$

and the total number of photons incident on the FPA in a time period T is simply

$$N = \Phi T = [P / (hc / \lambda)] * T \quad (10)$$

Hence the power exiting the fiber needed to yield N photons incident on the FPA in a time period T is

$$Pf(N,T) = N^* (hc / \lambda) / (q^*T) . \quad (11)$$

Choosing N = 1e5, T=30 msec, λ = 633 nm, and given q = 9.6e-4, yields

$$Pf(1e5, 0.030) = 1.1 \text{ nW}$$

This power is quite low for common solid state optical sources. However, it can easily be obtained for an optical source with nominally higher output power by defocussing the coupling between the source and the optical fiber. If necessary, T can also be reduced so that the total power reaching the FPA does not saturate the array. **Figure 7** shows the Pf required to provide 250,000 photons at the FPA (a number consistent with the FPA used in War Horse)for three different wavelengths in the VIS/NIR/SWIR range. We conclude that it will be straightforward to obtain appropriate values of Pf.

We note that, due to the small mode field diameter of the fiber and the possibly narrow spectral width of the optical source, it is quite possible that all of the light entering the

HSI foreoptics will fall entirely on one pixel. The calculation above, in fact, assumed that all the light entering the HSI was incident on one pixel.

B. Reflective Method for Laboratory Boresighting

The general features of a reflective, laboratory boresighting system are shown in **Fig. 8**. The optical power returned through arm D of the fiber coupler will be maximized when the reflecting surface is perpendicular to the optical axis of the collimated beam. This method, in and of itself, only provides boresighting in pitch and yaw angles, not roll.

Calculation of the returned optical power proceeds in similar fashion to the calculation for P_{HSI} given above. Let Ar be the area of the reflecting surface and assume Ar <<Aa. Then the optical power reflected back toward the telescope P_r is given by an equation of exactly the same form as Eq. (7) except with q modified by replacing the area of the entrance aperture of the HSI with the area of the reflector

$$P_r = q' * Pf \qquad (12)$$

where

$$q' = (NA_t / NA_f)^2 * [\, Ar /((pi/4)*(D^2 - D'^2))] \,. \qquad (13)$$

Since the numerical aperture of the telescope is smaller than that of the fiber, and if losses in the telescope can be ignored, then the optical power exiting port D of the 2x2 50:50 coupler is

$$P_D = (1/2) * \tau * P_r \qquad (14)$$

where the factor 1/2 comes from the coupler splitting ratio and $\tau < 1$ is the Fresnel power transmittance value. For light at normal incidence to a boundary between refractive indices n1 and n2,

$$\tau = 1 - [(n1 - n2) / (n1 + n2)]^2 \qquad (15)$$

For an air-silica interface, n1 = 1.0 (air), n2 = 1.46 (silica) and, hence $\tau = 0.96$.

We found a significant problem with this approach due to the relatively high level of outgoing light that is reflected from both the fiber endface and from the flat surface of the corrector plate. For example, The Fresnel power reflectance value for the same air-silica interface is

$$R = 1 - \tau = [(n1 - n2) / (n1 + n2)]^2 = 0.04 \qquad (16)$$

By comparison, assuming a reflecting surface of area equal to the area of the input aperture of the HSI, the fraction of outgoing light returning from the reflecting surface is approximately 0.001. Hence, the optical power reflected from the fiber endface is 40

times larger than the light returning from the reflecting surface. It will be difficult to distinguish the "true" signal riding on top of a background signal forty times as large. What is needed is a way to unambiguously distinguish the true reflected signal from any stray reflected signal. With some additional hardware, this can be accomplished as shown in **Fig. 9.** Here, a mechanical chopper is placed directly in front of the signal reflector and the optical signal returned to port D of the coupler is analyzed using a phase sensitive detector (lock-in amplifier). Since only the optical signal of interest is modulated by the chopper, it is easily distinguished from the large, but steady, background signal.

Expected Accuracy of Laboratory Boresighting Method

Regardless of pixel size in the CCD array, the fundamental limit to any measurement of spatial variations in the object is determined by the diffraction limit. For a circular entrance pupil of diameter D, a perfectly collimated beam of spatially incoherent light incident on the input aperture produces at the image plane a distance f from the input aperture, an intensity distribution given by square of the Airy function

$$I(x,y) = I_o\left[\frac{2J_1(q)}{q}\right]^2 \qquad (17)$$

where

$$q = \pi(D/\lambda)(r/f)$$

$I_o = (\pi D^2/4\lambda f)^2 I_{in}$ is the peak intensity

$$r = \sqrt{x^2 + y^2}$$

and J_1 is the Bessel function of the first kind of order 1. The square of the Airy function is plotted in **Fig 10.** Zeros of J_1 occur at q = 3.8317, 7.0156, 10.1735. The central disk of radius $r_c = 1.22(\lambda d/D)$ contains approximately 84% of the total intensity (and 91% of the total intensity is contained within the first two disks. The diameter of the central disk is often referred to as the diffraction "blur spot" and is specified in angular terms as

$$\theta_{diff} = 2*1.22(\lambda/D) \qquad (18)$$

and in terms of linear dimension as

$$2r_{diff} = 2*1.22(\lambda * f\#) \qquad (19)$$

where the f-number $f/\# = d/D$ is the ratio of the focal length to the diameter of the entrance pupil. **Figure 11** shows the blur spot diameter as a function of wavelength for various f-stop values. Hence, for an f/2.8 spectrometer with collimated, monochromatic input light at 633 nm, the blur spot diameter is approximately 4.3 um, well within the 14 um pixel size.

For simplicity, we assume a one-dimensional model and calculate the relative optical power in the central pixel (containing the center of the blur spot) and the adjacent two pixels as shown in **Fig. 12** as the center of the blur spot is moved corresponding to angular misalignment of the optical axis. With only 256 bits pixel depth for War Horse in the unbinned settings, it is seen that the offset must reach at least 4-5 um to produce a few bits change in pixel output. To be conservative, we can choose 6 um offset, corresponding to approximately 10 bits change, as an easily discernable change in pixel value. The angular deviation corresponding to 6 um is (6 um/14um)*280 urad = 120 urad. Hence, we conclude that it will be possible to align the War Horse system to the direction of a collimated beam to within approximately 120 urad, or slightly less than 1/2 pixel.

Clearly this boresighting system can align pitch and yaw but not roll. Work is in progress to develop a laboratory method for aligning the roll angle between two or more sensors.

Summary

We have discussed both a field method and a laboratory method for boresighting two or more optical sensors for airborne reconnaissance and surveillance applications. Both methods rely on human judgement by the operator although the laboratory method could be automated easily. The field method relies on vertical and horizontal boundaries in the far-field of the optical systems and should achieve rms alignment error in the range 485-970 urad. The laboratory method relies on collimated light produced using a fiber optic source and a telescope and should achieve rms alignment error of approximately 120 urad, a factor of approximately four better than the best case field alignment.

A future technical report will deal with the issue of thermo-mechanical stability of the mechanical frame.

The following table summarizes the performance characteristics of several sensor systems.

Table 2

Parameter	*Symbol*	**Dalsa**	**War HORSE**	**IRON HORSE**
Scan Configuration	-	Line Scan	Push-broom	Push-broom
Spectral range	-	VIS	VIS/NIR	NIR/SWIR
Wavelength range(nm)	λ_2–λ_1	400-1000	400-1000	900-2350
Slit width (um)	W	10	12, 25	18
Slit height (mm)	H	60	19	18.3
FPA		6000x1	1024x1024	Rockwell HgCdTe/TCM 8600 1024x1024
# spectral bands (unbinned)	Nb	1	64	504 (168 @ 3:1 bin)
Unbinned band width (nm)		400-1000	11.4	17
f/# (Front optics)	f/#	f/4 - f/22	f /2.8	f/2.8
f/# (Spectrometer)	f/#	na	f/2.0	f/2.8
Focal length (mm)	*f*	200	50-55	64.3
Input Aperture (mm)	D	50 (f/4) 9 (f/22)	30	35
Full Field of View (deg)	FFOV	17.1	16.3	16.3
Full Field of View (urad)	FFOV	2.98e5	2.84e5	2.84e5
Instantaneous FOV(urad)	IFOV	50	280	280
# x-track pixels	nx	6000	1024	1024
# d-track pixels	nd	1	(~slit width)	(~slit width)
FPA pixel pitch (um)	δ	10	14	18
FPA pixel size (um x um)		10 x 10	14 x 14	18 x 18
Max Frame rate (Hz)	FRmax	240(usable) 5k (max)	50	35-120
Ext FR trigger?		no	yes	no
Digitization(bits)		8	12	14

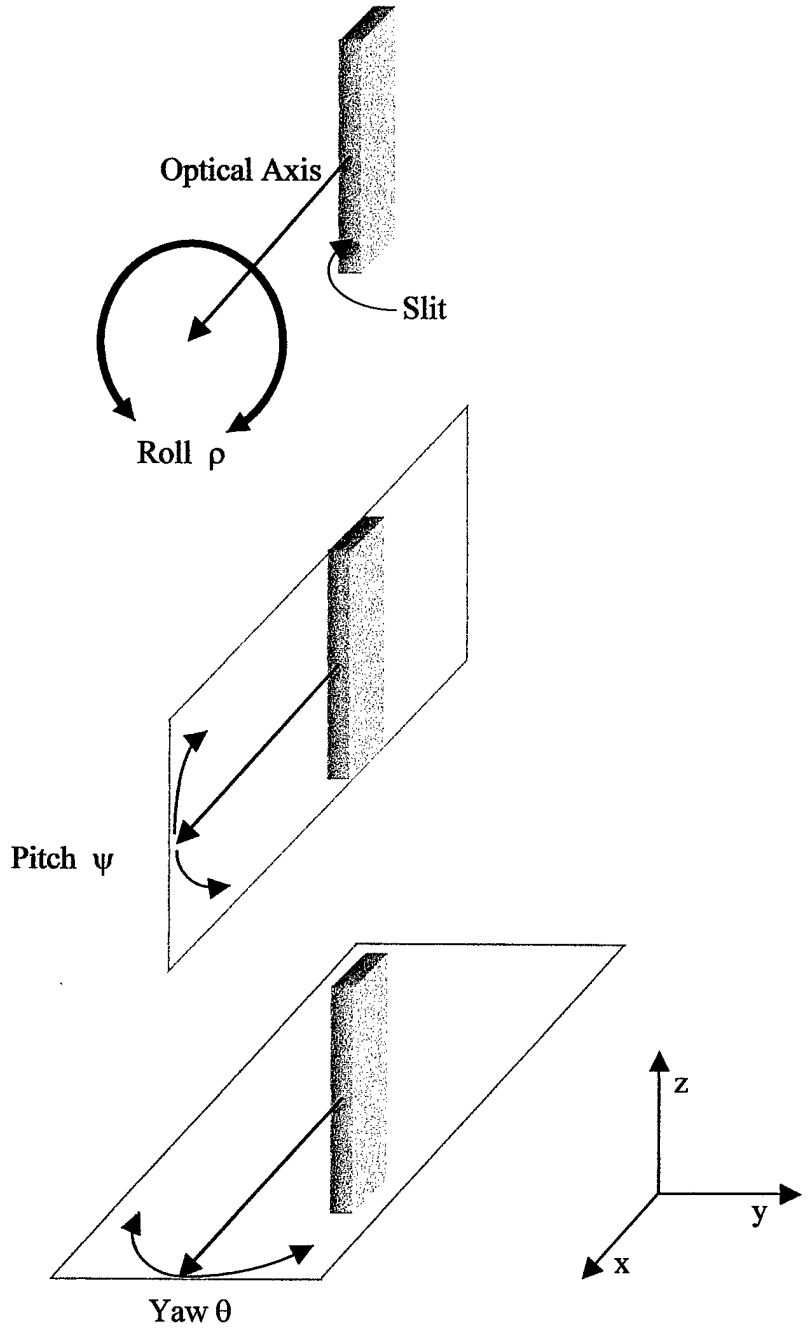

Fig. 1. *Angular degrees of freedom with respect to the optical axis.*

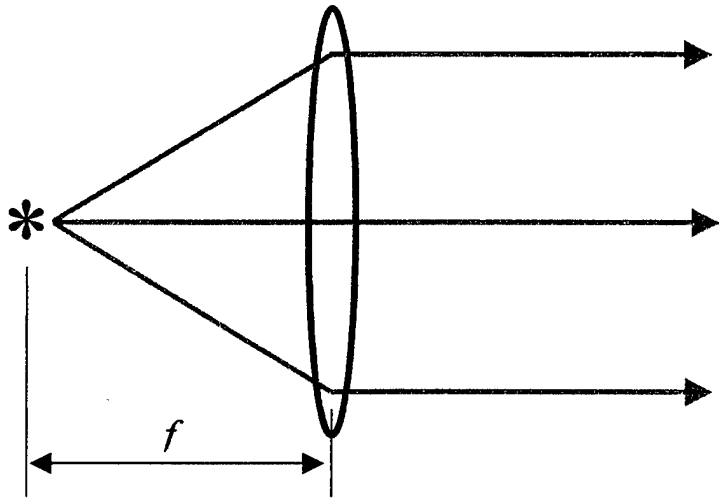

Fig. 2. *Production of collimated light using a point source at the focal point of a positive lens*

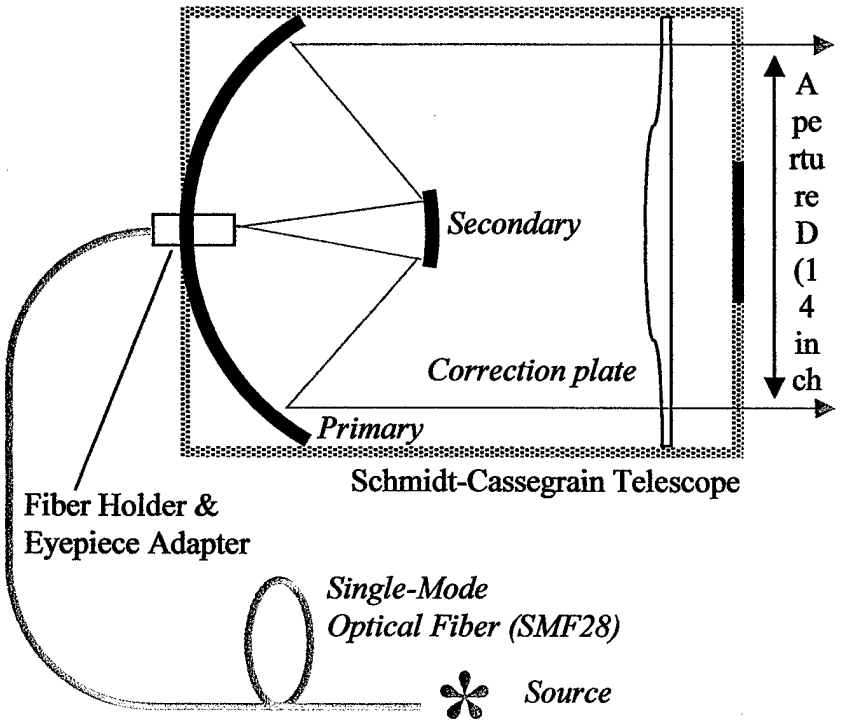

Fig. 3. *Singlemode optical fiber coupled to a Schmidt-Cassegrain telescope*

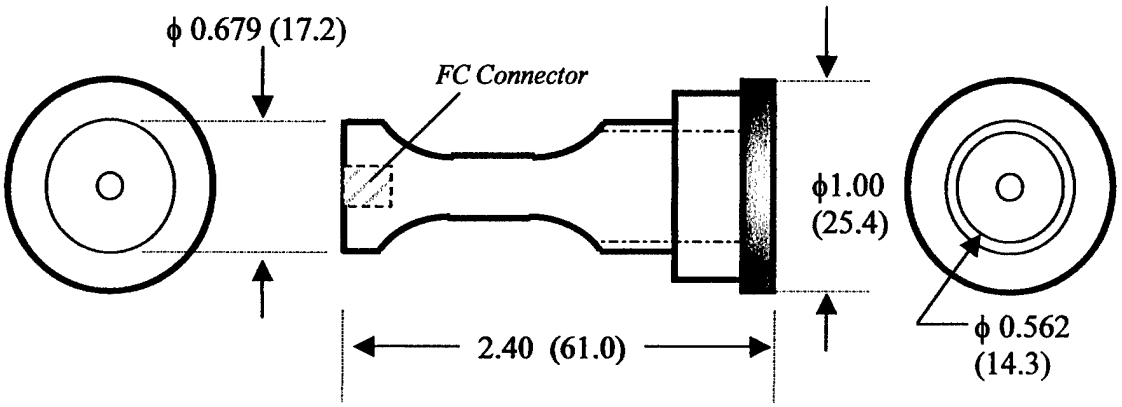

Fig. 4. *Newport Model FPH-CA4 fiber chuck holder*

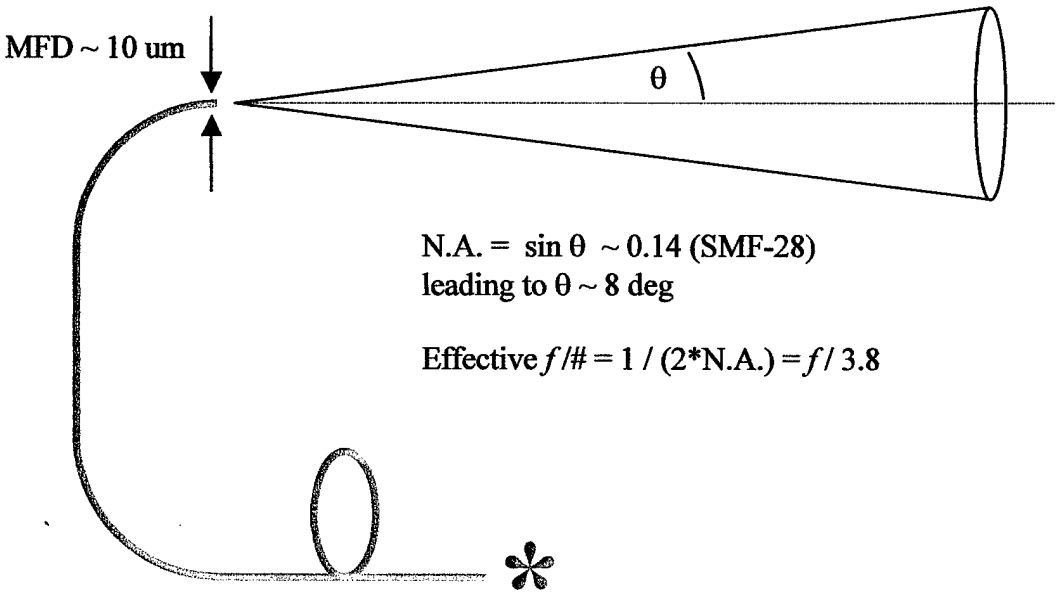

Fig. 5. *Exit optics for the singlemode fiber*

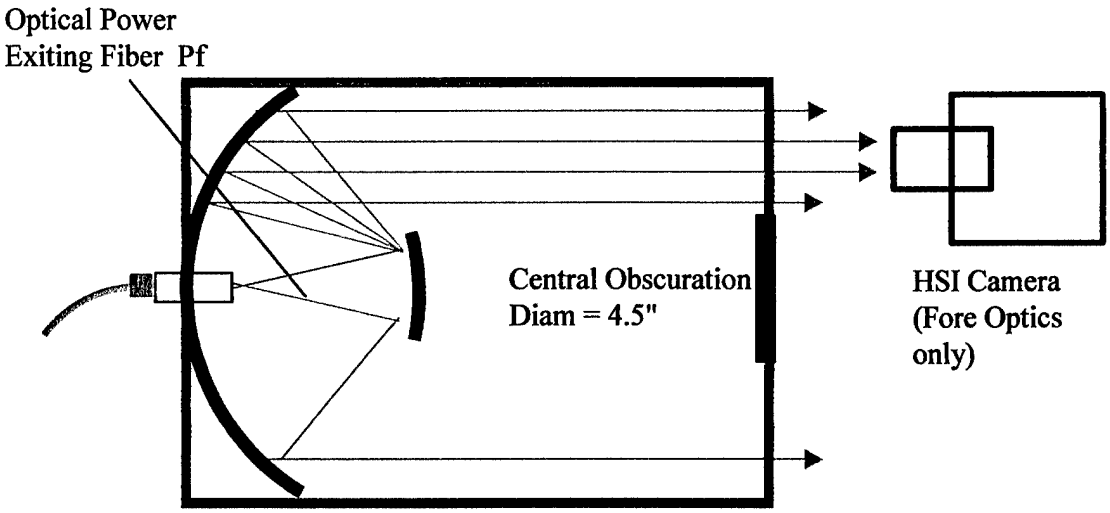

Fig. 6(a). Illumination of the HSI

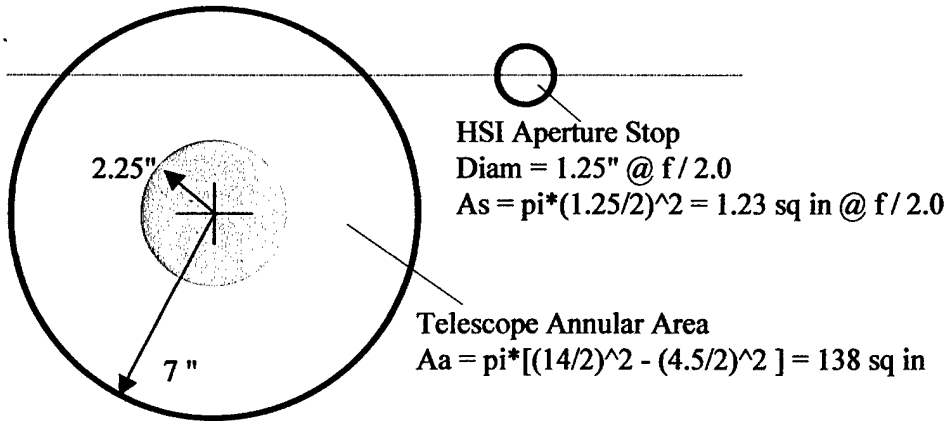

Fig. 6(b). Relevant areas.

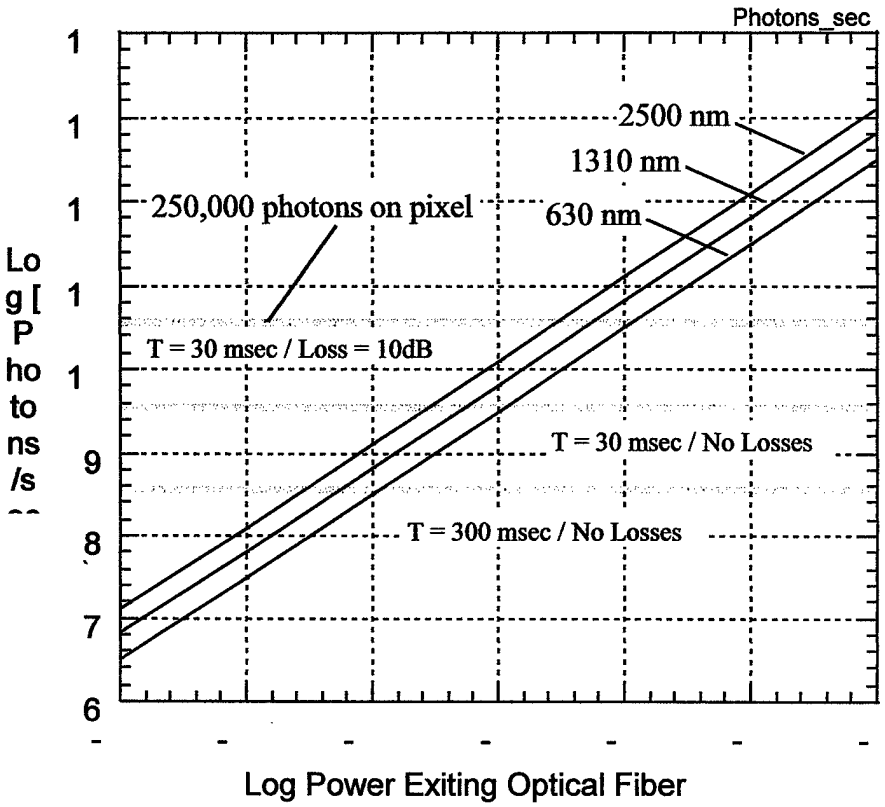

Fig. 7. *Power exiting fiber needed to provide 250,000 photons at FPA under various assumptions of integration time T and system loss. Required power for a given wavelength occurs at the intersection of the wavelength line and the flat 250,000 photons line.*

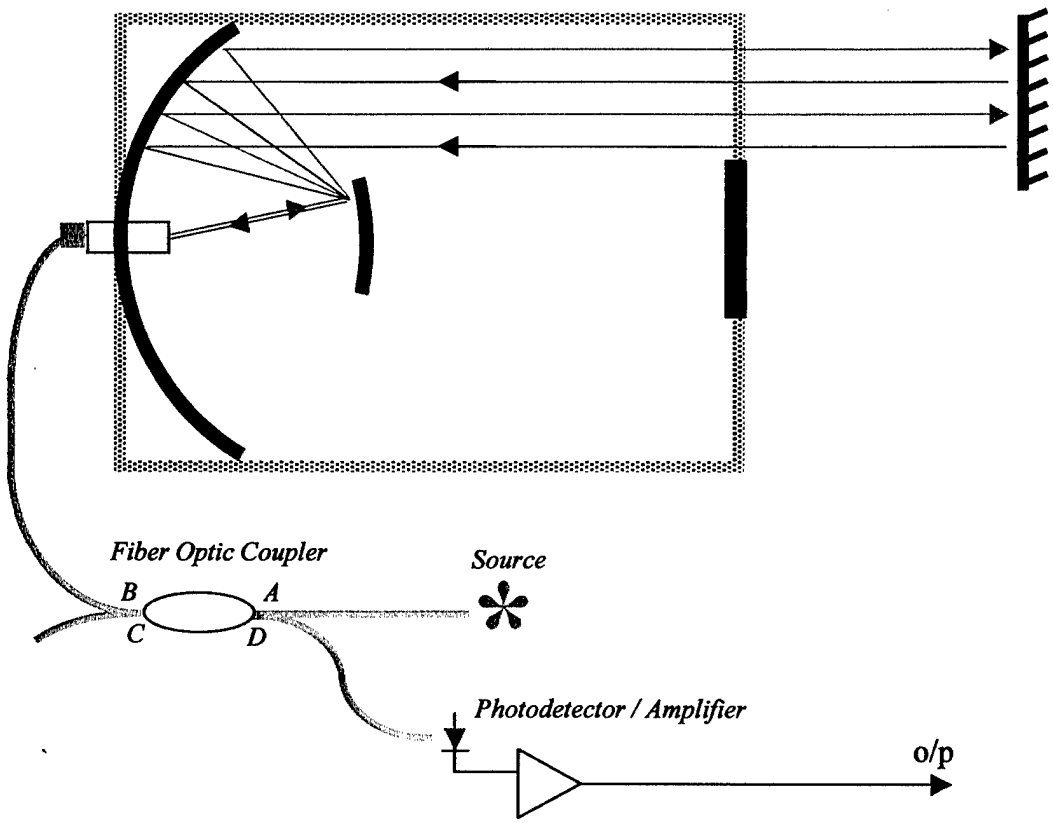

Fig. 8. *Use of a fiber optic coupler to direct outgoing light to the telescope and reflected (incoming) light to a photodetector.*

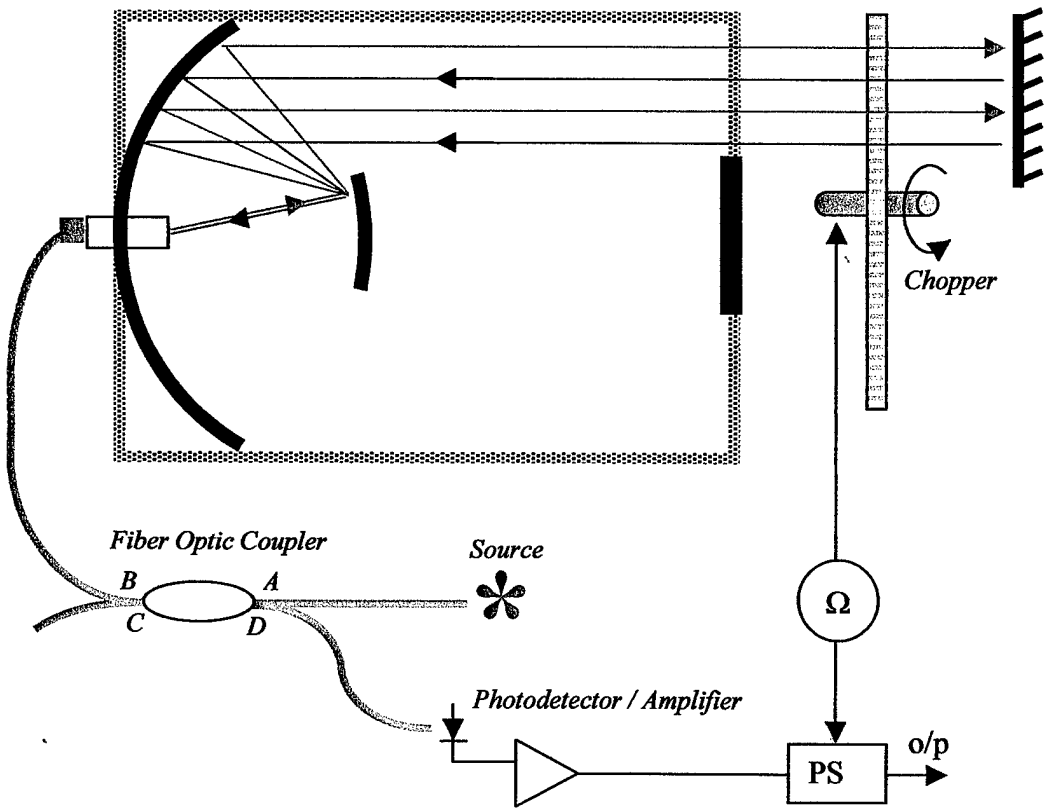

Fig. 9. *Addition of a chopper and phase-sensitive detector (PSD) to mitigate the effects of unwanted reflected light.*

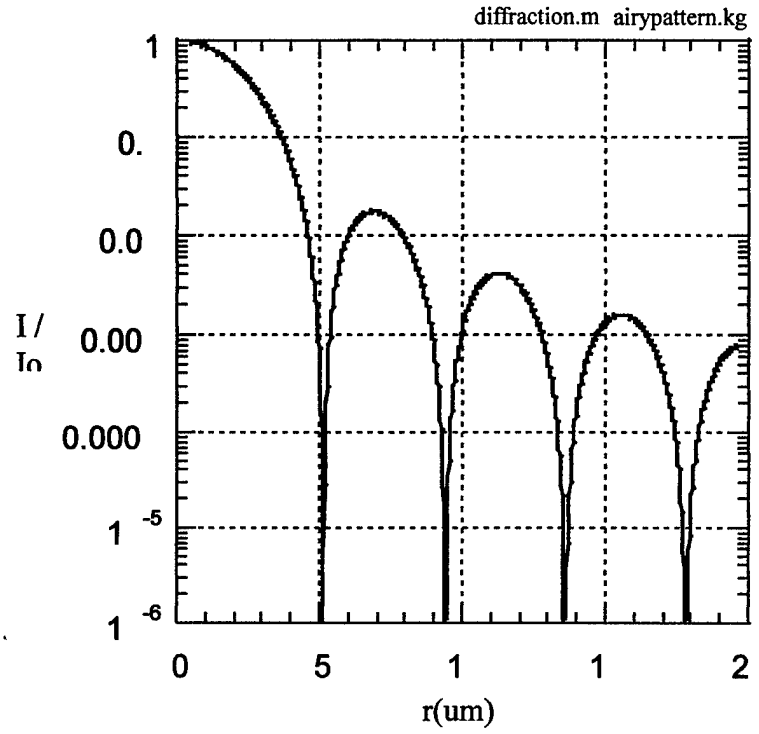

Fig. 10. *Airy pattern for a system with d/D = f/# = 2.8 operating at λ= 1.5 um. Approximately 84% of the power is contained within the λcentral disk, and 91% of the power is contained within the first two disks.*

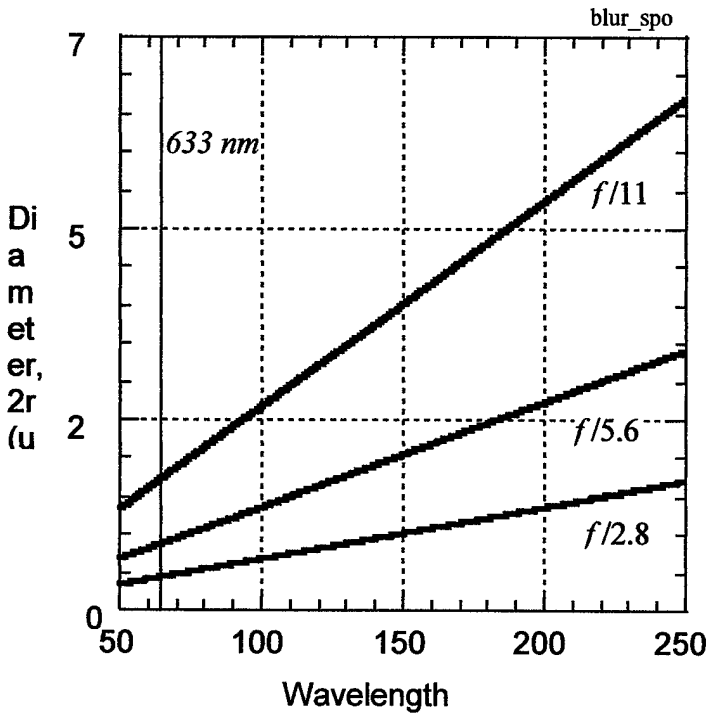

Fig. 11. *Diameter of the diffraction-limited blur spot as a function of wavelength for various f-stop values.*

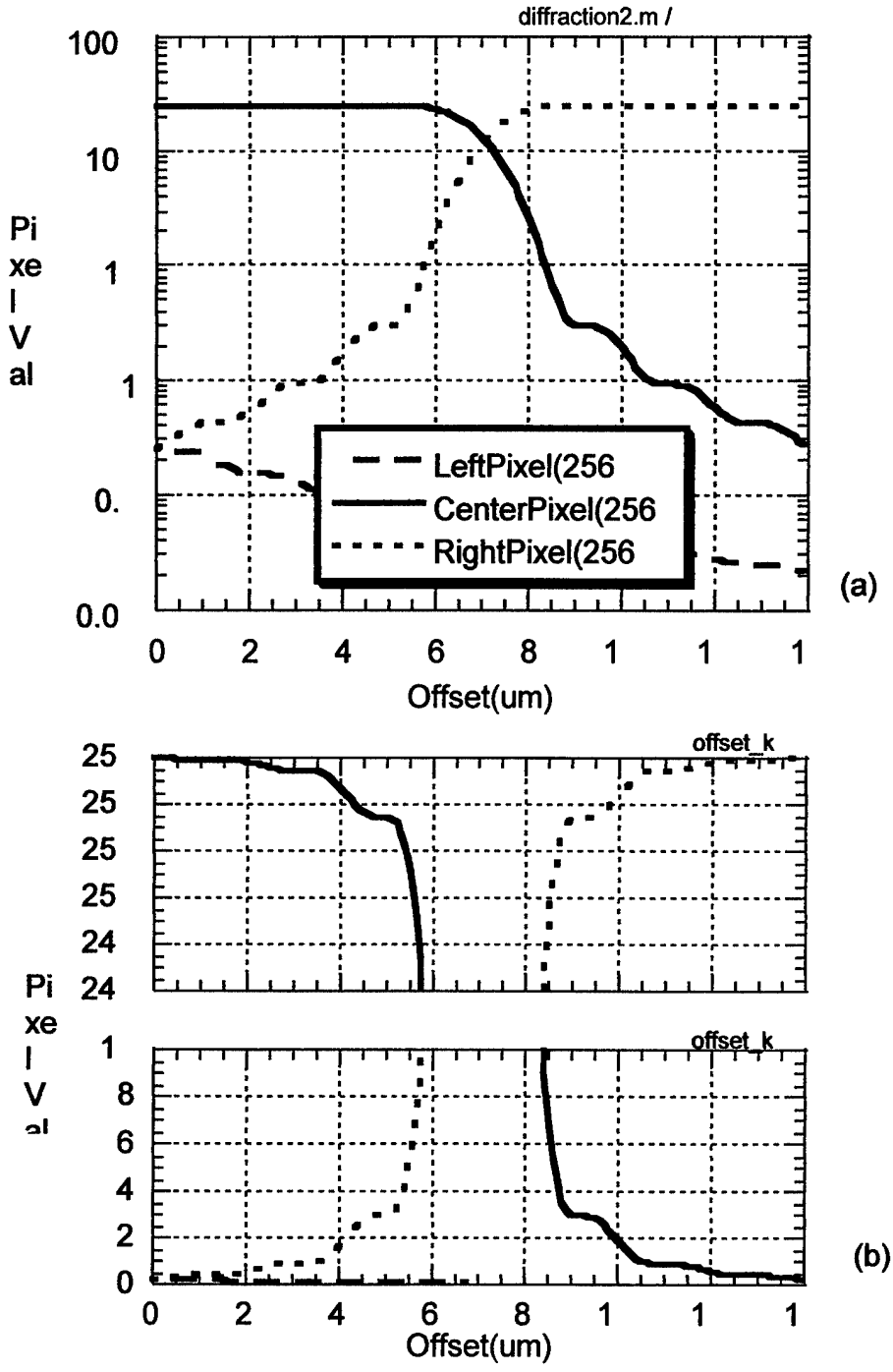

Fig. 12. (a) *Variation in light level on center and two adjacent pixels, measured in bits, assuming the optical power is adjusted to completely fill the 8-bit unbinned capacity of the WarHorse CCD array.* ***(b)*** *Detailed view near the top and bottom of the range.*